JACS
JOURNAL OF THE AMERICAN CHEMICAL SOCIETY
pubs.acs.org/JACS
Article

Design of Large Stokes Shift Fluorescent Proteins Based on Excited State Proton Transfer of an Engineered Photobase

Elizabeth M. Santos,[‡] Wei Sheng,[‡] Rahele Esmatpour Salmani, Setare Tahmasebi Nick, Alireza Ghanbarpour, Hadi Gholami, Chrysoula Vasileiou, James H. Geiger,* and Babak Borhan*

Cite This: *J. Am. Chem. Soc.* 2021, 143, 15091−15102
Read Online
ACCESS | Metrics & More | Article Recommendations | Supporting Information

ABSTRACT: The incredible potential for fluorescent proteins to revolutionize biology has inspired the development of a variety of design strategies to address an equally broad range of photophysical characteristics, depending on potential applications. Of these, fluorescent proteins that simultaneously exhibit high quantum yield, red-shifted emission, and wide separation between excitation and emission wavelengths (Large Stokes Shift, LSS) are rare. The pursuit of LSS systems has led to the formation of a complex, obtained from the marriage of a rationally engineered protein (human cellular retinol binding protein II, hCRBPII) and different fluorogenic molecules, capable of supporting photobase activity. The large increase in basicity upon photoexcitation leads to protonation of the fluorophore in the excited state, dramatically red-shifting its emission, leading to an LSS protein/fluorophore complex. Essential for selective photobase activity is the intimate involvement of the target protein structure and sequence that enables Excited State Proton Transfer (ESPT). The potential power and usefulness of the strategy was demonstrated in live cell imaging of human cell lines.

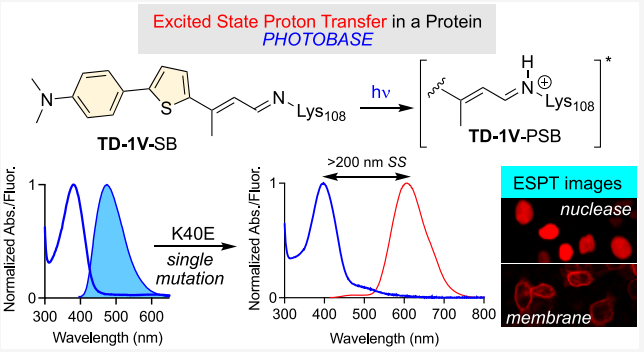

INTRODUCTION

Fluorescence microscopy has revolutionized many areas of biomedical research. These range from fundamental studies of *in vivo* protein−protein interactions, protein trafficking and single molecule nanoscopy to a wealth of other biological processes including whole body imaging and clinical applications in companion diagnostics such as ISH (*in situ* hybridization).[1] The available toolkits that enable various technologies within the field include fluorescent proteins (FPs)[1a,g,2] and proteins that are post-translationally modified by synthetic dyes.[1e,3] Together, these FPs provide emission spectra spanning the visible spectrum from the blue to the near-infrared (NIR).[1c,2d,4] The spectral diversity of fluorescent reporters enables multicolor imaging, wherein multiple target proteins and/or organelles can be visualized in a single microscopic experiment.[4a,5]

The evolving field of fluorescence microscopy has demanded newer, more sophisticated FPs to address deficiencies of the early generation candidates. While the ideal system might be case dependent, optimization of a set of photochemical characteristics is common to all; namely, photostability, red-shifted emission, high fluorescence quantum yield (QY), high extinction coefficient (ε), and large Stokes shift (≥100 nm). Recently, the design of FPs with "apparent" large Stokes Shift (LSS) has garnered attention.[6] These proteins display a large gap between the excitation and the emission maxima. Although Stokes shift is defined as the electronic transition between the excited and ground state of the *same chemical entity*, LSS-FPs achieve their *apparent* large Stokes shift by a chemical conversion of the excited state to a new bathochromic species, with a corresponding red-shifted emission. The large Stokes shift of these FPs is advantageous for their application in fluorescence imaging, since the wide gap between the excitation and emission maxima diminishes self-absorption. This not only minimizes the inner-filter effect, but is also beneficial in multicolor imaging experiments, wherein potential cross-talk between multiple emitters is reduced. If properly designed, a LSS emitter can be excited in the visible range of the electromagnetic spectrum while it emits in the near-infrared region. This additional feature further benefits imaging experiments by reducing light scattering, increasing signal depth in tissues, and eliminating autofluorescence. Although large Stokes shift and high fluorescence efficiency are not mutually exclusive, they are generally not encountered together in synthetic probes.

Received: May 15, 2021
Published: September 13, 2021

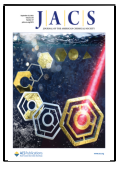

Fluorochromes with certain features are known to have increased Stokes shifts. Examples are molecules that can undergo intramolecular charge transfer (ICT) upon excitation,[7] form excimers/exciplexes,[8] or those that are affected by the Stark effect.[9] The application of these molecules as fluorescence imaging probes, however, is challenging in the practical sense—nonspecific targeting of ICT emitters leads to broad emission in the biological milieu, while incorporating an imaging trigger for the exciplex can be challenging. Alternatively, molecules that undergo excited state transformations circumvent these limitations; the absorption of species *A* can lead to a transformation of the excited state to form species *B*, the consequent emission of which does not constitute the same electronic transition; thus a large "apparent" Stokes shift is achieved (Figure 1a). This design

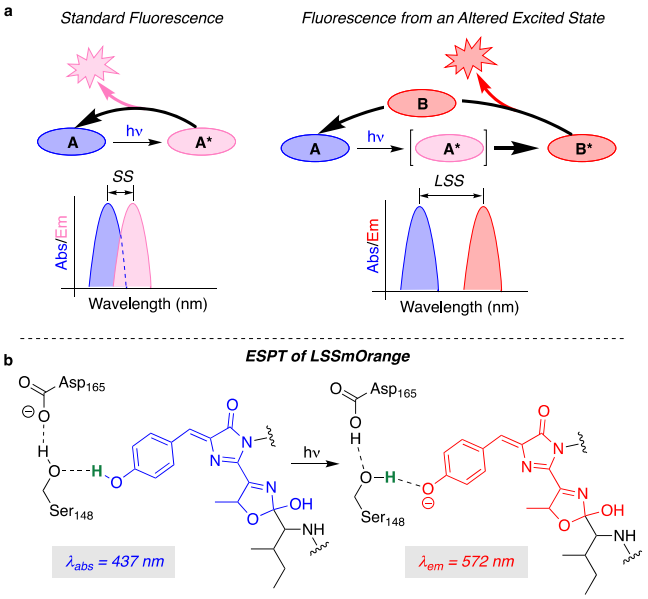

Figure 1. (a) Model for a large Stoke shift (LSS) system, as compared to standard fluorescence. Conversion of the excited state species **A*** to a bathochromically distinct molecule **B*** leads to the emission from a red state, resulting in a large Stoke shift; (b) The ESPT mechanism for LSSmOrange as a photoacid, excited at 437 nm, with emission observed at 572 nm.

strategy gives more flexibility to the selection of fluorochromes as well as an easier incorporation into host−guest systems such as a protein−ligand complex that mimics fluorescent proteins or other post-translationally modified tags. Perceivably, this will allow for an easier imaging application, welcomed by a broader community of cell biologists.

An example of the latter strategy is the case of excited state proton transfer (ESPT). This strategy has been successfully implemented in the GFP lineage, as well as for small synthetic fluorescent molecules. The former is represented by a series of LSS-FPs such as LSSmOrange, LSSmKates, mKeima, CyOFP1, and mBeRFP, to name a few.[10] Operationally, the intrinsic fluorophores for all these FPs, the core *p*-HBI, remains neutral in the ground state, while nearby amino acid residues are engineered to engage in hydrogen bonding with the phenolic hydroxyl group (Figure 1b). Upon light irradiation, the acidity of the phenolic species in the excited state increases by orders of magnitude (lowering the pK_a), enabling the proximal amino acid residue(s) to initiate a proton abstraction, which may or may not occur through a proton relay. The resultant phenolate, with its enhanced conjugation, relaxes through a red-shifted emission that leads to an apparent large Stokes shift. Critical for its success is the placement of a hydrogen bond acceptor in proximity to the phenolic hydroxyl to facilitate the ESPT. Reports have shown Asp, Glu, Asn, and Lys are good hydrogen bond acceptors for this purpose.[10]

Small molecules that possess an appropriate hydrogen bonding donor and acceptor, oriented in a suitable position and distance within the same molecular framework, can also yield a large apparent Stokes shift through internal ESPT, or ESiPT (Excited State intramolecular Proton Transfer).[7a,11] The first reported example is salicylic acid, described by Weller in the 1950s.[12] Since the original report, a variety of molecular families capable of the ESiPT process have been reported. Common hydrogen bond acceptors in these systems include benzimidazoles, benzoxazoles, benzothiazoles, quinolines, flavones, chromenes, and anthraquinones.[13] To furnish the ESiPT process, a carbonyl or other relevant heteroatom hydrogen bond acceptor is proximal to a phenol moiety within the same molecule. A number of ESiPT capable molecules are constituent elements for various chemosensors and chemidosimeters to probe biologically or environmentally important chemical species.[11a]

To date, all reported ESPT-capable FPs and ESiPT-capable small molecules function as photoacids—molecules that experience decreased pK_a and lose a proton in the excited state. In fact, most reported ESPT small molecules are photoacids as well, with only a few known photobases.[14] In contrast to photoacids, photobases are able to extract a proton in their excited states. In our own work, we have previously reported a fluorene-based super photobase, **FR0**-SB, which is capable of deprotonating a primary or secondary alcohol, exhibiting a ΔpK_a greater than 14 units. The protonation of the photobase leads to an Intramolecular Charge Transfer (ICT) system, red-shifted in the excited state, leading to a > 250 nm apparent Stokes shift (Figure 2a).[15] The latter discovery piqued our interest for the possibility of incorporating a fluorophoric photobase into a rationally engineered protein carrier, with the goal of generating a photoactivatable LSS-FP. The plan would require appropriate positioning of amino acid side chains to facilitate the required proton source for the photobase. To the best of our knowledge, this design strategy, which utilizes photobases instead of photoacids, is unique and could have advantages in generating highly conjugated polar ICT systems in the excited state that are well red-shifted in emission, with high QY.

Herein, we demonstrate the engineering of a small protein receptor, which forms an imine through the reaction of specifically designed aldehydic ligands with an active site lysine residue. Photoexcitation of the protein/fluorophore complex leads to ESPT, presumably as a result of the protonation of the imine nitrogen atom via a nearby residue, judiciously placed to deliver the proton. The subsequent generation of an iminium in the excited state, evident from the apparent large Stokes shift in emission, highlights the photobasic ability of the protein/fluorophore complex. The following describes the design of the protein binding pocket, as well as the structural requirements of the chromophore, to yield a protein/fluorophore complex that exhibits a large apparent Stokes shift in excess of 200 nm, and fluorescence quantum efficiencies >70%. To the best of our knowledge this is the

https://doi.org/10.1021/jacs.1c05039
J. Am. Chem. Soc. 2021, 143, 15091−15102

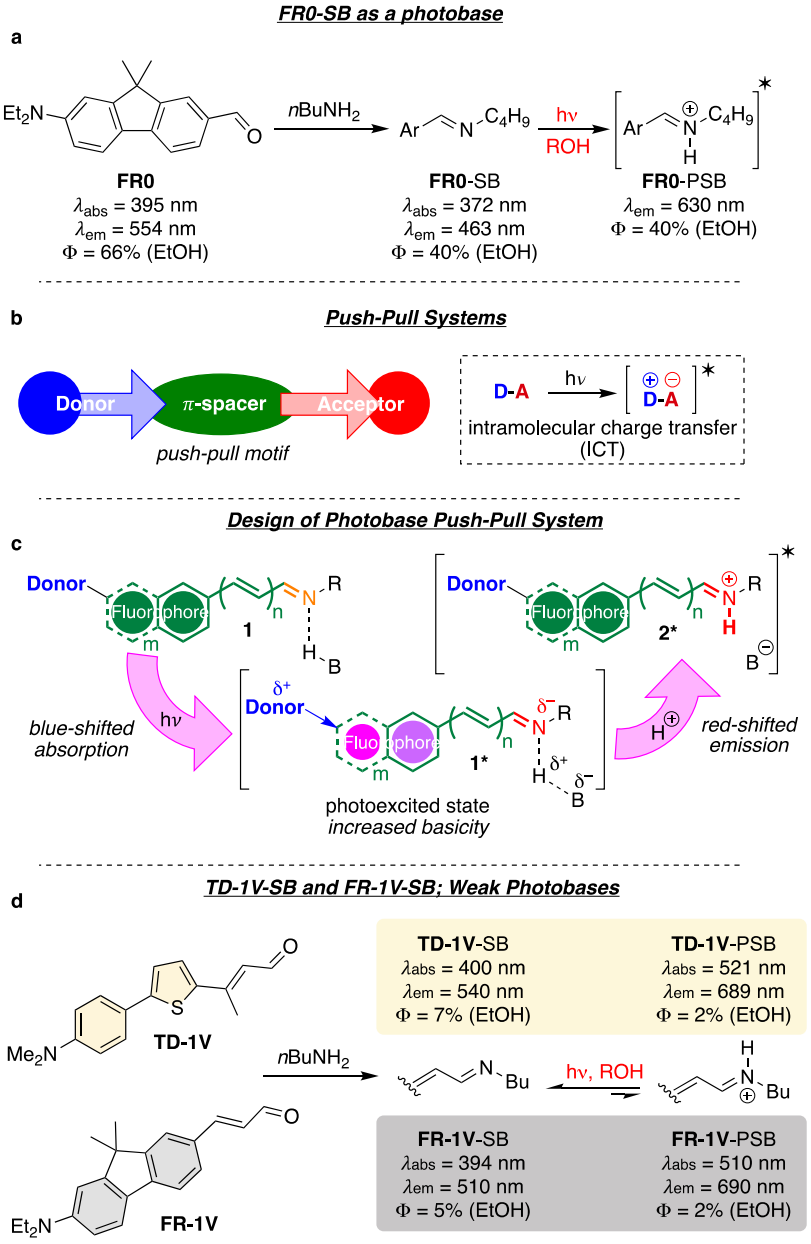

Figure 2. (a) The Schiff base of **FR0** (**FR0**-SB) is a strong photobase, emitting as **FR0** protonated Schiff base (**FR0**-PSB) in the excited state; (b) photoexcitation of push−pull systems can lead to dramatic redshift absorptions as a result of internal charge transfer (ICT); (c) illustrated is the design principle for a photobase capable of ICT. The aromatic spacers behave as "circuit breakers", which are triggered open by photoexcitation. The charge redistribution increases the basicity of the imine, leading to a red-shifted ICT system; (d) the imine of **TD-1V** (**TD-1V**-SB) and **FR-1V** (**FR-1V**-SB), are weak photobases ideal for the proposed studies.

first example of a photobase active protein system. The photophysical characteristics of an LSS fluorescent protein complex would lay the groundwork for a new protein-labeling paradigm for imaging and detection.

RESULTS AND DISCUSSION

General Consideration for an ESPT-Capable Chromophore. We envisioned that the photoexcitation of an appropriately engineered protein/fluorophore complex could lead to an ICT species. Photobasicity would result from localizing electron density on the electron-withdrawing (acceptor) moiety in the excited state. With an appropriately long excited state lifetime, the increased electron density, and thus increased basicity, could result in protonation of the acceptor. The protonation event would yield a red-shifted fluorophore, hence an LSS system. As depicted in Figure 2b, an ICT system is composed of an electron donor, a π-spacer, and an electron acceptor. We opted for the scenario shown in Figure 2c, where the effective electron acceptor (the iminium) is not present in the ground state. In an operative system, photoexcitation of the protein complex **1** will lead to an increase of the imine's basicity (**1***) in the excited state, and the subsequent protonation would generate an excited state iminium (**2***), producing the requisite electron acceptor for a functional ICT system.

On the basis of our prior protein engineering work on rhodopsin protein mimics, we opted for an aldehydic molecule that would form the requisite imine upon reaction with an

https://doi.org/10.1021/jacs.1c05039
J. Am. Chem. Soc. 2021, 143, 15091−15102

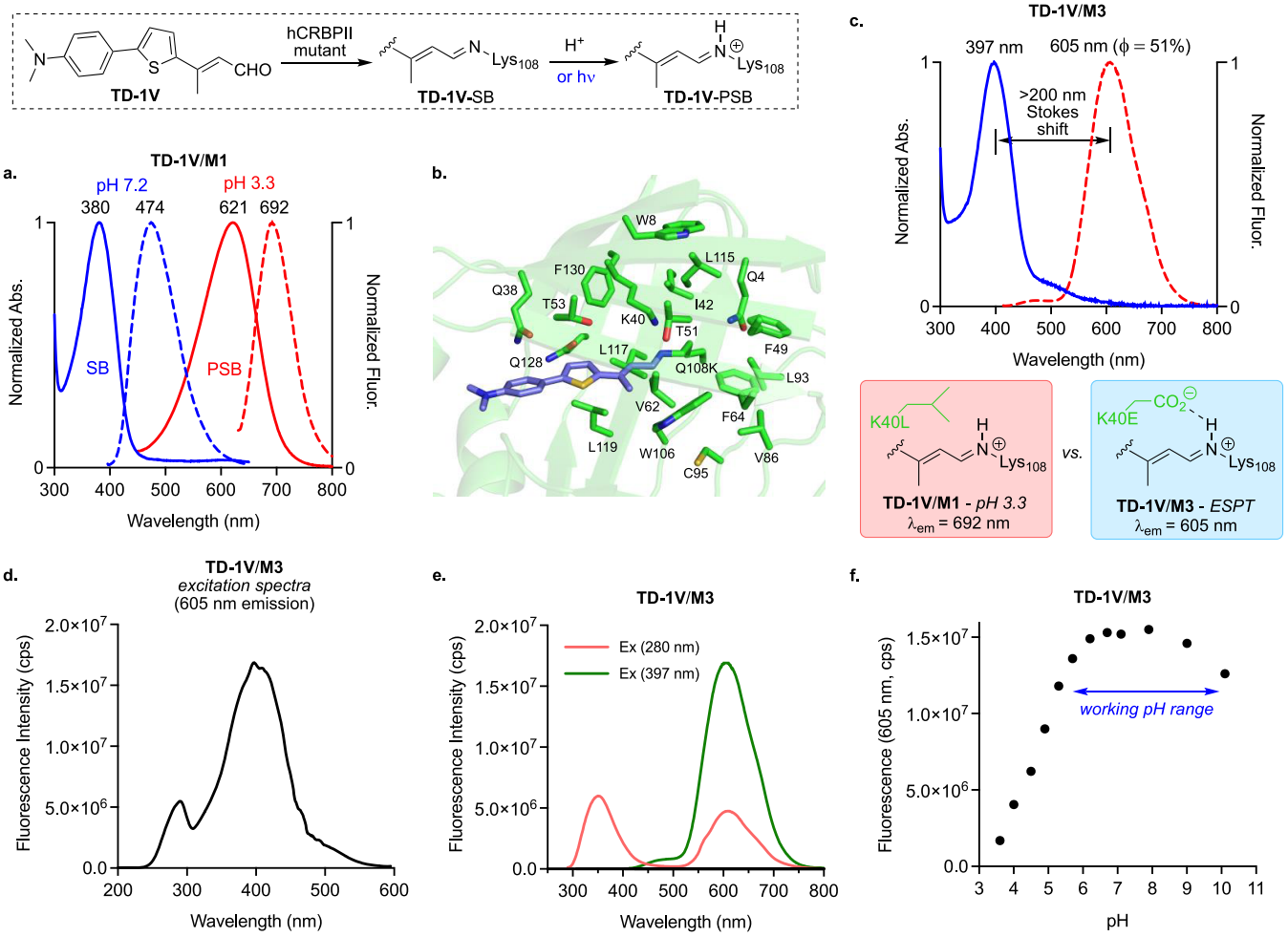

Figure 3. (a) UV−vis and fluorescence spectra (380 nm excitation) of **TD-1V**/**M1** complex at pH 7.2 leads to SB emission at 474 nm, while the acidified sample (pH 3.3) is red-shifted to 621 nm (PSB form), with emission at 692 nm; (b) energy minimized structure of **TD-1V**/Q108K-hCRBPII complex with selected residues within 10 Å of the imine nitrogen atom highlighted; (c) UV−vis and fluorescence spectra (397 nm excitation) of **TD-1V**/**M3** complex, exhibiting ESPT emission with >200 nm Stokes shift. Comparison below figure highlights the reason why the ESPT generated iminium is blue-shifted relative to the iminium generated via acidification of the media; (d) excitation spectrum of the **TD-1V**/**M3** complex (emission observed at 605 nm); (e) emission spectra of **TD-1V**/**M3** complex, excited at 280 and 397 nm; and (f) emission of the **TD-1V**/**M3** complex incubated at various pH values, exhibiting a pH working range (∼5−10) of the pigment with high emission output.

active site lysine residue in the protein host.[16] Our work with the super photobase **FR0**-SB (*vide supra*) provided the structural requirements for generating an ICT system; an electron donor appendage (diethylamino group), a π-spacer (fluorene), and an electron acceptor unit (imine). Yet, **FR0**-SB was not considered as a promising candidate because of its strong activity as an ESPT capable fluorophore, which we deemed detrimental in achieving selectivity and low background. Thus, we opted for an imine system that exhibited weak ESPT in protic solvents. This may seem counterintuitive; however, it is imperative that the iminium is generated in the excited state, and only in the binding cavity of the engineered target protein; namely, the protein host should play a critical role in the proton transfer event. This ensures that nonspecific imine formation in the biological milieu is inconsequential, since ESPT is only possible in the designed protein environment. In this manner, it should be possible to achieve selectivity, as emission of the iminium is only observed in the target protein.

Another route to heighten selectivity is to accelerate protein/fluorophore maturation kinetics relative to nonspecific imine formations. A properly oriented protic amino acid residue may not only facilitate ESPT to the imine, but could also accelerate imine formation through hydrogen bonding with the aldehydic oxygen. In fact, we have previously shown that the incorporation of a single acidic residue can lead to >26 fold rate enhancement in imine formation.[16c] The rapid imine formation with the protein target differentiates it from nonspecific reactions in the biological milieu, such that the fluorescence from the target protein dominates, hence resulting in negligible background. Finally, the ability to control the pK_a of the resultant imine in the binding pocket of the target protein is key, since ESPT is impossible if the imine is already protonated in the ground state.

In line with the structural requisite for an ESPT-capable ICT dye, we selected a panel of fluorophores that contained a push−pull scaffold for ligand/protein complex engineering. These included a Dapoxyl analog with red-shifted emission and high quantum yield (**TD-1 V**, Thio-Dapoxyl with 1 vinyl appendage, Figure 2d),[17] and derivatives of **FR0** with reduced photobasic ability (see below for structures, and Table S6 of the Supporting Information, SI, for photochemical details).

https://doi.org/10.1021/jacs.1c05039
J. Am. Chem. Soc. 2021, 143, 15091−15102

Table 1. Spectroscopic Properties TD-1V/hCRBPII Mutant Complexes

mutant	hCRBPII mutant[a]	λ_{abs}	$\lambda_{em\ (SB)}$	$\lambda_{em\ (PSB)}$	Φ^{b}	Φ_{ESPT}
M1	Q108 K:K40L:T53A:R58L:Q38F:Q4F	379	474	n.d.	0.03	<0.02
M2	Q108 K:K40L:T53A:R58L:**Q38E**:Q4F	389	485	n.d.	0.05	<0.02
M3	Q108 K:**K40E**:T53A:R58L:Q38F:Q4F	397	n.d.	605	0.51	>0.99
M4	Q108 K:K40L:T53A:R58L:Q38F:Q4F:**I42E**	406	n.d.	603	0.41	0.97
M5	Q108 K:K40L:T53A:R58L:Q38F:Q4F:**T51E**	399	n.d.	602	0.12	0.86
M6	Q108 K:K40L:**T53E**:R58L:Q38F:Q4F	387	480	n.d.	0.04	<0.02
M7	Q108 K:K40L:T53A:R58L:Q38F:Q4F:**V62E**	386	474	598	0.08	0.27
M8	Q108 K:K40L:T53A:R58L:Q38F:Q4F:**L117E**	391	486	653	0.13	0.73
M9	Q108 K:K40L:T53A:R58L:Q38F:Q4F:**L119E**	384	479	n.d.	0.05	0.13
M10	Q108 K:K40L:T53A:R58L:Q38F:Q4F:**Q128E**	385	473	n.d.	0.05	<0.02
M11	Q108 K:**K40E**:T53A:R58W:Q38F:Q4F:Y19W	392	n.d.	621	0.43	>0.99
M12	Q108 K:**K40D**:T53A:R58L:Q38F:Q4F	393	481	639	0.34	0.81

[a]20 μM protein and 0.5 equiv **TD-1V** at pH 7.2. [b]Absolute quantum yield was measured on a Quantaurus-QY. Not detected (n.d.).

Early evaluation focused our attention on **TD-1 V**, as well as **FR-1 V**, a homologue of **FR0**, both of which demonstrated spectroscopic characteristics that were on par with those described above, i.e., fluorophoric molecules capable of forming an ICT system upon Schiff base formation, yet with depressed photobase activity in protic solvents. Comparing the emission of **FR0**-SB with that of **FR-1 V**-SB in ethanol, it is quite evident that the former leads largely to the emission from the iminium via ESPT, while the latter displays only a small portion of fluorescence resulting from ESPT (Figure S1, see trace in EtOH, Table S7). A further check on **TD-1 V**-SB shows an even smaller portion of its fluorescence arising from ESPT (see Figure S1, trace in EtOH). The project now required a protein capable of binding the ligands as an imine with an active site lysine residue. Further engineering of the protein's active-site cavity would be required to not only ensure a low pK_a for the imine (to avoid protonation in the ground state), but also judiciously place amino acids relative to the position of the fluorophore to promote high levels of ESPT within the binding pocket.

Protein Reengineering. **TD-1V** was chosen as the starting ligand for protein reengineering. As described in detail below, our efforts focused on the reengineering of human Cellular Retinol Binding Protein II (hCRBPII), a small (136 aa), cytosolic protein with high expression yields and excellent structural resiliency, as a host for the fluorogenic dyes.[16a,18] Our prior work in this area has provided the required insight for reengineering this family of proteins.[16a−d,19] Most critical for the success of any protein engineering effort, is the robustness of the protein structure to numerous mutations. In our studies with over 500 mutants, hCRBPII has proven itself as a durable and structurally robust protein.

Introduction of a Glutamic Acid Residue as Proton Donor. Investigations to find an appropriate protein host for **TD-1V** began with the Q108K:K40L double mutant of hCRBPII. Prior studies have shown that these two mutations are critical for binding an aldehydic chromophore,[16a] albeit requiring optimization for each ligand family. Q108K serves as the active-site lysine for reaction with the aldehyde, while the K40L mutation presumably removes interactions between Q108K and Lys40 that is detrimental to imine formation. Addition of **TD-1V** to Q108K:K40L-hCRBPII led to the formation of the iminium, although the protein/fluorophore complex was not stable and its UV−vis spectrum was broad and featureless (Figure S2). After extensive structure-guided screening (see SI and Figure S3 for details), we arrived at the Q108K:K40L:T53A:R58L:Q38F:Q4F-hCRBPII hexamutant (**M1**), which in part had followed parallel reengineering efforts utilizing retinal as a ligand.[16a,20] The three hydrophobic mutations (T53A, R58L, and Q38F) were introduced to increase binding affinity and enhance the rate of pigment maturation. The Q4F mutation typically increases soluble protein expression, but more importantly, aids in suppressing the pK_a of the iminium, ensuring that the ground state system is populated solely as the imine.

M1 binds **TD-1V** as a SB in PBS buffer (pH = 7.2), as evident by its blue-shifted absorption (λ_{abs} = 380 nm, pK_a = 5.1) Excitation at 380 nm led to the predominant emission of the imine at 474 nm (Figure 3a). Incubation of **TD-1V**/**M1** complex in acidified PBS buffer (pH 3.3) yields the protonated SB, with absorption at 621 nm. Excitation at the latter wavelength leads to emission at 692 nm. The absorption and emission values for the ground state SB and PSB for **M1** define the anticipated spectroscopic regions for each state. We surmised that a nearby acidic residue could provide the necessary proton for a weak photobase, and thus, 19 residues proximal to the putative imine nitrogen atom were individually mutated to Glu (Q4, W8, Q38, K40, I42, F49, T51, T53, V62, F64, V86, L93, C95, W106, L115, L117, L119, Q128, and F130, Figure 3b). Residues as far as 10 Å from the imine were examined, owing to the possibility that ESPT could occur as a result of remote hydrogen bonded water networks (through proton relays). Unfortunately, a number of the mutants led to insoluble protein expression. Nonetheless, soluble protein was obtained after placement of Glu at nine positions (K40, T51, V62, I42, L117, T53, L119, Q38, and Q128) in the parent mutant **M1**.

The absorption spectra of **TD-1V**/hCRBPII mutant complexes can have two maxima, depending on the pK_a of its corresponding imine. The engineered sequences favored mutants with low pK_a, such that the ground state species could be protonated in the excited state. The excitation of the SB in these complexes can lead to two emission maxima, corresponding to fluorescence from the neutral (~480 nm) or the protonated imine (>600 nm) in the excited state as a result of ESPT. Figure 3c depicts the UV−vis spectrum of **TD-1V**/**M3** complex with absorption maximum at 397 nm, corresponding to its SB form (pK_a 5.2, see Figure S4 for pK_a measurements). Excitation of the complex at 397 nm leads to fluorescence centered at 605 nm, red-shifted far beyond the anticipated region for emission of the SB. Apparently, Glu40 is incapable of protonating the imine in the ground state to any

https://doi.org/10.1021/jacs.1c05039
J. Am. Chem. Soc. 2021, 143, 15091−15102

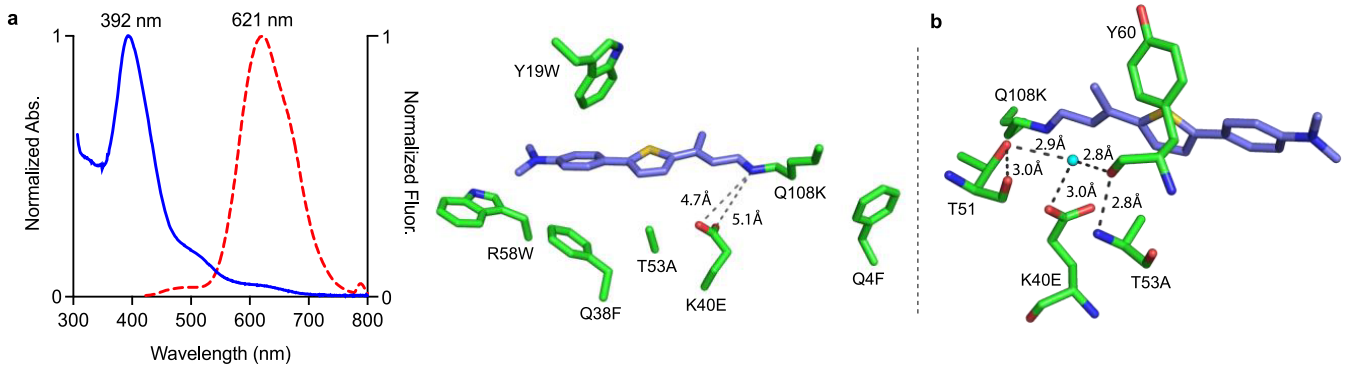

Figure 4. (a) UV−vis, fluorescence (>99% ϕ_{ESPT}), and crystal structure of **TD-1V/M11** complex. The imine nitrogen atom is ∼5 Å from Glu40, which is presumably the proton source for the formation of the iminium upon photoexcitation; (b) highlighted is the water molecule that interacts with K40E and the main chain carbonyl of Y60 and T51. These interactions lead to the proposition that the K40E side chain is protonated in the ground state, poised to deliver the proton to the imine upon excitation.

appreciable extent, yet, upon photoexcitation, the enhanced basicity of the imine triggers proton transfer to yield the iminium, which relaxes partly through fluorescence, followed by proton loss.

The blue-shifted emission of the **TD-1V/M3** complex (605 nm) relative to the protonated **TD-1V/M1** complex (692 nm) warrants explanation. The change in emission reflects the interaction of the Glu40 anion, generated after proton transfer, leading to a charge stabilized ion-pair that localizes the cationic charge on the nitrogen atom. This reduces the conjugation of the positive charge along the π-system, and consequently yields the blue-shifted emission. This speculation arises from our prior work that demonstrated the same phenomena in absorption regulation of rhodopsin protein mimics, where a salt bridge interaction at the iminium led to blue-shifted absorptions.[16a] In comparison, the **TD-1V/M1** complex, acidified to a pH of 3.3, leads to the same iminium, yet lacking the anionic interaction that would localize charge on the nitrogen atom. The observed red-shift is due to the greater delocalization of the positive charge along the polyene.

Emission data, obtained upon excitation of the SB at its absorption maximum for the nine mutants discussed above, are listed in Table 1. We defined Φ_{ESPT} as the fraction of the total fluorescence that originates from the excited state iminium. Briefly, the fluorescence spectrum was deconvoluted to give separate traces representing the emission from the neutral and protonated imine, respectively. The area under each deconvoluted peak was integrated to provide the relative percentage of total fluorescence quantum yield. The value derived from the iminium is defined as Φ_{ESPT} (see Figure S5 for a representative example for spectral deconvolution and calculation of Φ_{ESPT}). Consequently, larger Φ_{ESPT} values denote a more facile ESPT process.

High Φ_{ESPT} values were obtained for hCRBPII/**TD-1V** complexes that possess either K40E, I42E, or T51E mutations (Table 1, **M3**, **M4**, and **M5**), highlighting efficient ESPT of the imine ($\Phi_{ESPT} \geq 0.86$). Among the latter mutants, high fluorescence quantum yields were observed for **M3** and **M4** (0.51 and 0.41, respectively), while a pronounced reduction was observed for **M5** (0.12). On the basis of numerous crystal structures of this series of proteins in the PDB, the putative positions of all three residues are in close proximity (∼5 Å) to the imine nitrogen atom. Variants with V62E and L117E (**M7** and **M8**, respectively) lead to a significantly lower Φ_{ESPT}, with emission that results from both the chromophore's SB and PSB forms in the excited state; the remaining mutants led to typical SB emission as the major fluorescing event.

The excitation spectrum of the **TD-1V/M3** complex, collected at 605 nm, verifies that the observed fluorescence originates from the SB (Figure 3d). Interestingly, the excitation spectrum also shows an absorption at ∼280 nm, which presumably belongs to the Trp residues in hCRBPII. As a confirmation, excitation of the protein complex at 280 nm leads to peaks at both the expected SB and ESPT emissions of the bound chromophore. This observation suggests the existence of an energy transfer process from tryptophan to the bound **TD-1V**-SB (Figure 3e).

ESPT for the **TD-1VM3** complex is observed over a wide range of pH values, as shown in Figure 3f. Fluorescence emission is maximal at pH 6−9 and drops at more acidic or more basic pH values. At pH 10, the blue-shifted peak (emission of the SB) appears at <500 nm, presumably as a result of the deprotonation of the glutamic acid at position 40, and/or a less active bound water molecule as a proton donor. One would assume that a system with a stronger ICT would yield a more basic excited state capable of ESPT. At pH values below 5, the imine is protonated, and thus incapable of ESPT. If necessary, the working window can be adjusted based on the pK_a of the ground state iminium. We have previously shown that the pK_a can be adjusted through sequence alterations of the binding pocket in a rational manner.[19]

Structural Determinants of Optimal ESPT Variants. Sequence comparison of **M1** (not capable of ESPT) with **M3** (full ESPT) leads to the conclusion that the glutamic acid at position 40 must be responsible for providing the proton to the photobase upon photoactivation. Unfortunately, crystallization of the **TD-1V/M3** complex was not fruitful. Previous investigations with retinal as ligand had shown that the inclusion of two additional Trp residues at positions 19 and 58 results in a more ordered chromophore in the binding pocket. This inspired the Q108K:K40E:T53A:*R58W*:Q38F:Q4F:*Y19W* (**M11**) variant, which gave similar ESPT spectroscopic results (Table 1) and readily produced well-diffracting crystals suitable for structural analysis. The structure shows that the Glu40 carboxylate oxygen atoms are ∼5 Å from the imine nitrogen atom (Figure 4a), too far for direct interaction. A direct imine carboxylate interaction would likely lead to an iminium at physiological pH, which would be incompetent for ESPT. The conformation of Glu40 is defined by water-mediated interactions with the side chain of Thr51 and the

https://doi.org/10.1021/jacs.1c05039
J. Am. Chem. Soc. 2021, 143, 15091−15102

mainchain carbonyl of Tyr60 (Figure 4b). We surmised that both Thr51 and Tyr60 act as hydrogen bond acceptors to the water molecule, since Thr51 is also hydrogen-bonded to its own mainchain carbonyl. This would suggest that Glu40 is protonated and participates as a hydrogen bond donor for the water molecule. More importantly, the ground state structure corroborates the lack of any observable PSB at pH 7.2, since Glu40 maintains its proton as a result of the latter interactions In fact, the same interactions could also stabilize Glu40 as it donates a proton during the ESPT process. The intervening region between the SB and the carboxylate is surrounded by hydrophobic residues, apparently increasing the Glu40 pK_a and excluding water from the region. Though this discussion assumes ESPT emanates from the fluorophore conformation observed crystallographically, other ESPT-competent fluorophore conformations cannot be ruled out.

The analogous Asp40 mutant also supports protonation of the excited state species, but with reduced efficiency (~80% transfer) and a higher imine pK_a (6.4 as compared to 5.2 for Glu40). The smaller SB population leads to less available imine for ESPT. At first glance, it seems counterintuitive that the shorter Asp side chain would lead to a higher pK_a of the bound **TD-1V**-PSB, as the longer Glu side chain should be closer to the imine, and thus enjoy enhanced electrostatic interactions. This piqued our interest in factors that not only affect the pK_a of the SB, but also could lead to more facile ESPT. Crystallographic analysis of the K40D variant indicates that the Asp40 side chain maintains a similar 5 Å distance to the imine, but does not make the water mediated interaction with Thr51 and Tyr60 seen with Glu40 (Figure S6). In contrast to Glu40, Asp40 can donate its proton to the imine, stabilizing the ensuing charge through ionic interactions, which leads to a higher pK_a. The pK_a's of the carboxylic acid and the iminium are coupled due to their proximity, thus the pK_a of the iminium is governed by its interactions with the carboxylate side chain. The reduced ESPT efficiency may be related to the absence of interactions that would stabilize the position of Asp40 (Figure S6). Furthermore, the K40D mutant **M12** produced a less stable protein product, and was prone to dimerization. Together these results are illustrative of how intricate water-mediated interactions lead to the low iminium pK_a and high ESPT efficiency required to optimize an LSS fluorescent protein.

Evaluation of Other Ionizable Residues. Because introduction of Glu or Asp at residue 40 leads to ESPT, we hypothesized that other residues may be able to support the ESPT process as well. Hence, as listed in Table 2, Glu40 was replaced in **M3** with other amino acids with proton-bearing side chains. Neither cysteine (**M13**) nor threonine (**M14**) led to ESPT upon excitation of the SB at physiological pH (Figure S7), and produced spectra similar to that observed for **M1** (K40L, see Figure 3a). However, substitution of basic residues histidine (**M15**), lysine (**M16**), and arginine (**M17**) in position 40 resulted in partial ESPT (Figure S8). Presumably, they either directly protonate the imine in the excited state, or they polarize a hydrogen bonded water molecule, which would function as the proton donor. Nonetheless, their Φ_{fl} were much lower than that observed with K40E (**M3**). A potential explanation is that the carboxylate counteranion, produced as a result of ESPT from Glu, has a stronger interaction with the iminium as compared to the iminium/amine pair, which results from ESPT with His, Lys or Arg. The ionic interaction may lead to chromophore rigidification and a higher quantum yield.

Table 2. ESPT of M3 Mutants at Position 40

mutant	residue 40[a]	λ_{abs}	$\lambda_{em\ (SB)}$	$\lambda_{em\ (PSB)}$	Φ[b]	Φ_{ESPT}
M1	K40L	379	474	n.d.	0.03	<0.02
M3	K40E	397	n.d.	605	0.51	>0.99
M13	K40C	383	480	n.d.	0.07	<0.02
M14	K40T	386	487	n.d.	0.13	<0.02
M15	K40H	393	477	642	0.09	0.50
M16	K40	389	491	661	0.08	0.40
M17[c]	K40R	392	492	653	-	0.43
M18	K40Q	388	488	663	0.11	0.11
M19	K40Y	393	495	674	0.04	0.14

[a]20 μM protein and 0.5 equiv **TD-1V** at pH 7.2. [b]Absolute quantum yield was measured on a Quantaurus-QY. [c]The QY of **M17** could not be obtained due to its inherent instability. Not detected (n.d.).

Similar to the basic residues, glutamine (**M18**) and tyrosine (**M19**) showed dual fluorescence bands (blue-shifted emission from the SB and red-shifted emission from the protonated excited state of the SB) with suppressed quantum yields (Figure S9).

Expansion of the Ligand Scope for ESPT. Inspired by the ESPT results obtained with **TD-1V**, we explored the efficiency of other ligands (**FR0**, **FR-1V**, **FR-2V**, and **FR-Th**) to elicit ESPT when complexed with **M3** (Figure 5). The

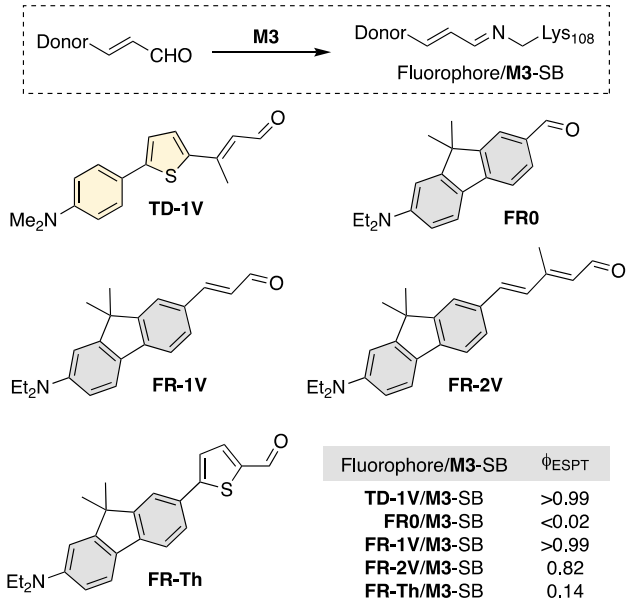

Figure 5. Structure of various ICT-capable fluorophores complexed with **M3** as a Schiff base (SB). **TD-1V** and **FR-1V** stand out with high ϕ_{ESPT} (>0.99).

characteristic ESPT long wavelength emissions were observed to various extent with **FR-1V**, **FR-2V**, and **FR-Th**, although the **FR-Th**/**M3** complex was not ideal, with low Φ_{ESPT} (0.14). Interestingly, the **FR0**/**M3** complex was not ESPT active, yet it exhibits full ESPT with an alternate mutant that contains K40D and V62E as potential proton donors (see Figure S10). This highlights the obligatory role of the protein host in providing a path for proton transfer, which also depends on the structure and trajectory of the bound molecule in the active site. Similar to **TD-1V**, the **FR-1V**/**M3** complex exhibits complete ESPT- with its long wavelength emission band centered at 595 nm (Φ_{ESPT} > 0.99), along with a surprisingly

https://doi.org/10.1021/jacs.1c05039
J. Am. Chem. Soc. 2021, 143, 15091−15102

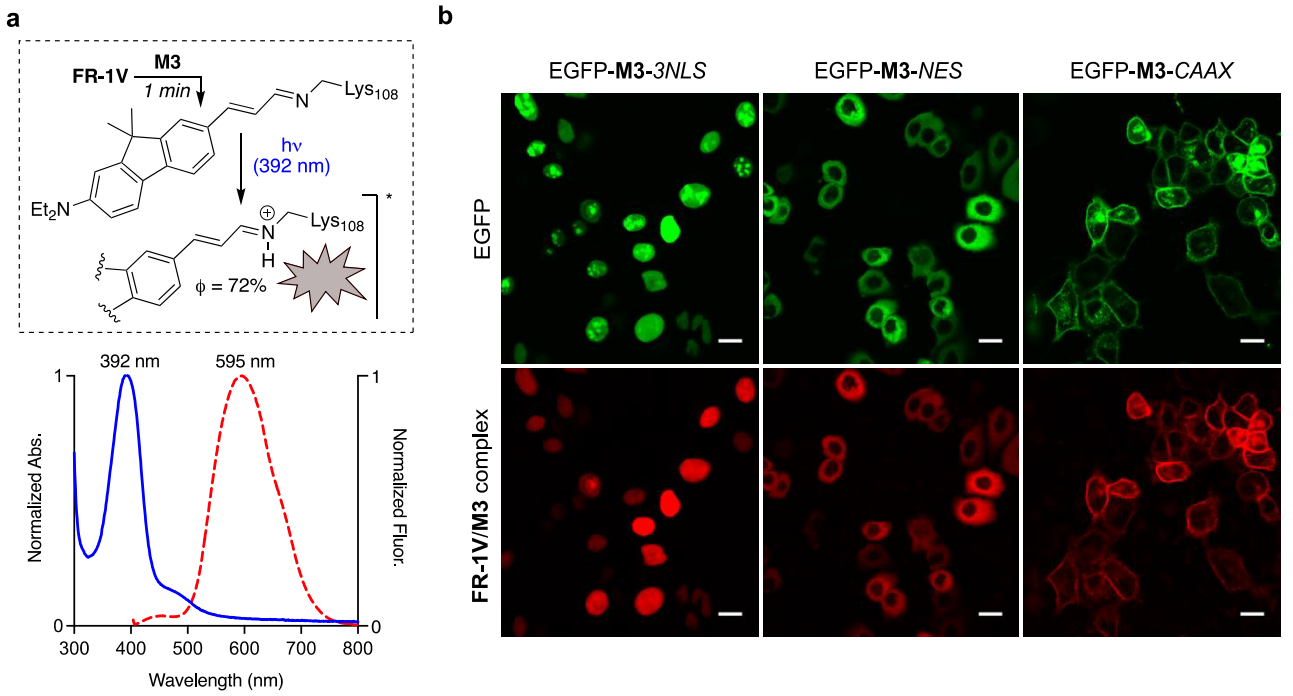

Figure 6. (a) **FR-1V** complexed with **M3** yields a SB in ground state (λ_{max} 392 nm, pK_a = 5.2). ESPT of the complex leads to emission at 595 nm; (b) compartmentalized **FR-1V**/**M3** imaging in live HeLa cells. NLS = nuclear localization sequence. NES = nuclear export sequence. CAAX = prenylation tag. Cells were stained with 500 nM **FR-1V** and incubated at 37 °C for 1 min. Cells were washed 3 times with DPBS before imaging. Scale bar, 10 μm.

effective fluorescence QY (72%), and an apparent Stokes shift of over 200 nm (Figure 6a). Its excitation spectrum also shows double maxima at 280 and 595 nm, respectively, as observed with **TD-1V**/**M3** (see Figure S11). This spectroscopic resemblance may be attributed to the similarity between **FR-1V** and **TD-1V** in terms of their molecular geometries, conformations within the protein cavity, and electronic structures. Not surprisingly, **FR-2V**, with its increased conjugation, led to a more red-shifted absorption for its SB and its corresponding ESPT emission when complexed with **M3** (405 and 663 nm, respectively). Nonetheless, ESPT emission suffered somewhat (Φ_{ESPT} = 0.82), likely as a result of its increased flexibility.

Though structures could not be obtained for any of the **FR** fluorophores bound to **M3**, the **FR-1V**/**M15** complex, differing from **M3** only at position 40 (K40H versus K40E in **M3**), produced well diffracting crystals. The latter complex exhibits the anticipated ESPT behavior, albeit less robustly, with the most significant issue being the prevalence of the iminium state at pH 7.2 (Figure S12). A possible explanation for the spectral properties is inspired by the structure of the complex (Figure S13). Two distinct conformations of K40H are seen in the four molecules that comprise the asymmetric unit. In two chains (A and B), K40H makes a direct interaction with the iminium nitrogen atom (3.0 Å), while in the other two chains (C and D), K40H rotates away, and instead makes a water mediated hydrogen bonded network with Gln128 and Arg35. Likely, K40H's direct interaction stabilizes the PSB (increased pK_a), explaining the significant amount of the protonated imine. Alternatively, in chains C and D, where the K40H is rotated away from the imine, the pK_a is suppressed, yet its proximity to the His residue accommodates ESPT. This is similar to that seen for **M11**-bound **TD-1V**, where Glu40 is nearby, but not directly interacting with the imine of the SB.

Live-Cell Imaging. Our next aim was to demonstrate that the utilization of the photobase-initiated ESPT process can complement current photoacid–based LSS design approaches. We chose the hCRBPII hexamutant **M3** for proof-of-principle live-cell imaging. As discussed earlier, it is critical to have a rapid binding event between the chosen aldehydic ligand and the protein host, such that its formation outcompetes other possible nonspecific binding within the biological milieu. This effectively minimizes background fluorescence from unintended sources. Initial screens with ligands was performed with a mixed order binding kinetic measurement. **M3** (20 μM) was incubated with selected ligands (10 μM) at room temperature. **TD-1V** and **FR-1V** exhibited fast binding kinetics with half-time of 1.5 min and 0.16 s, respectively (see Figure S14). We further measured the second order binding rate constant of **FR-1V** with **M3** (1.38×10^6 M^{-1} s^{-1}, see Figure S15 for detail). Cellular imaging with far-red/near-infrared emitting pigments is preferred because of their cleaner optical window, deeper penetration depth, and minimal fluorescence background. With the latter consideration in mind, along its superior photochemical characteristics, and rapid pigment maturity (Figure 6a), **FR-1V** was chosen for the proof-of-concept cell imaging assays.

Three different C-terminus appended constructs of **M3** cloned into a pFlag-CMV2 vector were prepared: (1) 3 × NLS tag (three sequential nuclear localizing sequences); (2) NES (nuclear export signal) tag; and (3) CAAX motif, for plasma membrane localization. All constructs contained an EGFP gene inserted at the N-terminus of **M3** to serve, not only as a control for transfection, but also as an indicator for colocalization with the ESPT fluorophore. HeLa cells transfected with the constructs described above were incubated with **FR-1V** (500 nM) for 1 min at 37 °C, washed 3 times to remove the dye containing media, and immediately subjected to imaging. The

https://doi.org/10.1021/jacs.1c05039
J. Am. Chem. Soc. 2021, 143, 15091−15102

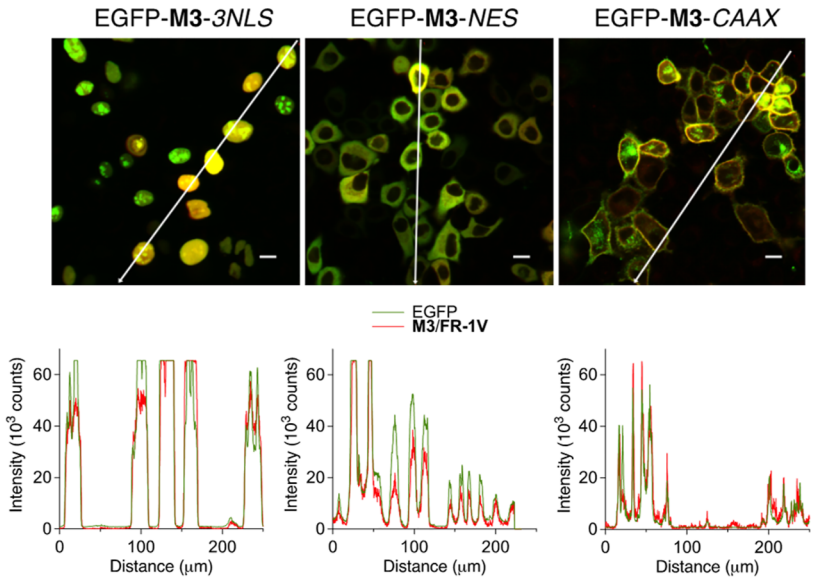

Figure 7. ESPT fluorescence specificity of **FR-1V/M3**. Top row shows the merged EGFP and LP615 channels of transfected live HeLa cells with **M3** localized in cell nuclei, cytosol, and plasma membrane, respectively. Bottom row shows the line profiles of colocalized EGFP and ESPT signal along the white arrows in the top images. Scale bar, 10 μm.

field of view was excited with a 405 nm LED laser, and the emission resulting from ESPT was collected through a 615 nm long-pass filter, non-ESPT based emitters. Even though the 615 nm long-pass filter (LP615 channel) essentially filters half of the ESPT emission band, the resultant images were bright, enabling fine structural visualization of labeled plasma membrane (see Figure 6b). To further examine the labeling and ESPT fluorescence signal specificity, the pixel profiles of EGFP and ESPT emissions from the two channels are superimposed in Figure 7. Since EGFP and **M3** were appended together, any nonoverlapping peaks in these line profiles would be the result of off-target labeling and background fluorescence. Happily, images of all three constructs showed no observable background fluorescence or nonspecific labeling. To our knowledge, the **FR-1V/M3** tag is brighter than any other LSS fluorescent proteins, and its labeling kinetics is faster than most of the known imaging tags/labels.[21]

To place this work in context, it is prudent to correlate the work presented here with our previously reported efforts with photoswitches.[16b] In prior work, the **FR-1V** fluorophore was used to conjugate with a different hCRBPII engineered mutant in a proof-of-principle demonstration of a no-wash live cell imaging in the near-infrared window. Comparable to the no-wash system, the ESPT system reported in this work also shows high specificity in our imaging model. Although both systems use the same fluorophore and mutants from the same protein scaffold, the underlying difference is in the photochemical mechanics. Critically, the previous no-wash system is realized via excited-state photoisomerization of a double bond, which leads to a positional change of the chromophore relative to the protein binding pocket, and subsequent *ground-state* proton transfer that yields the ICT system. Thus, the ground state is protonated, resulting in an emission with <100 nm Stokes shift. In contrast, the current rapid LSS system is realized via photobase-initiated *excited-state* proton transfer. The two systems together highlight the ability to synthetically tweak and control a given photochemical complex on the molecular level in a manner to alter its energy dissipation pathway on the surface of excited state and achieve desired functionalities (namely isomerization of a double bond or protonation in the excited state).

CONCLUSIONS

We demonstrate the conceptualization, rational design, and implementation of a new paradigm of LSS fluorescent probes utilizing photobasic fluorophores. Excited State Proton Transfer (ESPT) leads to emission of the protein host/fluorophore complex in the NIR region. The fluorogenic molecules undergo Intramolecular Charge Transfer (ICT) upon photoexcitation, leading to an increased electron density, and heightened basicity of the imine nitrogen atom. Engineered protein hosts are designed to not only bind the fluorogenic molecules as an imine, but also deliver a proton upon excitation to support the ESPT process. Such a photobase phenomenon is rarely seen, even in small molecules in solution. The ability to apply this phenomenon in a protein system opens new avenues in the development of photoactive and fluorescent proteins. Specifically, we have identified fluorescent ligands for engineered hCRBPII protein hosts capable of >200 nm apparent Stokes shift, maximal >70% fluorescence quantum yield, and close to unity ESPT emission ratio. Among these ligands, **FR-1V** was found to have superior fast-labeling kinetics and rapid cell permeation. In a proof-of-concept imaging assay, the **FR-1V/M3** complex exhibits the ability to fluoresce mammalian cells, at a wavelength 200 nm from it is excitation, with short incubation periods, high brightness, and excellent staining specificity. We speculate that this concept and design is general, readily applicable to imaging tag designs, and can be extended to much broader fields, including smart light-responsive materials, functional probes, and optogenetics.

ASSOCIATED CONTENT

Supporting Information

The Supporting Information is available free of charge at https://pubs.acs.org/doi/10.1021/jacs.1c05039.

https://doi.org/10.1021/jacs.1c05039
J. Am. Chem. Soc. 2021, 143, 15091−15102

Experimental data including synthesis of the fluorophores, protein expression and purification, UV−vis spectra, HPLC extraction, crystallization conditions, and X-ray data collection and refinement statics; crystallographic files such as atomic coordinates and structure factors have been deposited in the Protein Data Bank, www.pdb.org (PDB ID codes: 7LSQ, 7MFX, 7MFY, 7MFZ) (PDF)

AUTHOR INFORMATION

Corresponding Authors

James H. Geiger − *Michigan State University, Department of Chemistry, East Lansing, Michigan 48824, United States*; Email: geiger@chemistry.msu.edu

Babak Borhan − *Michigan State University, Department of Chemistry, East Lansing, Michigan 48824, United States*; orcid.org/0000-0002-3193-0732; Email: babak@chemistry.msu.edu

Authors

Elizabeth M. Santos − *Michigan State University, Department of Chemistry, East Lansing, Michigan 48824, United States*; Present Address: Dow Performance Silicones, 2200 W. Salzburg Rd, Midland, MI 48686

Wei Sheng − *Michigan State University, Department of Chemistry, East Lansing, Michigan 48824, United States*; orcid.org/0000-0002-9044-905X

Rahele Esmatpour Salmani − *Michigan State University, Department of Chemistry, East Lansing, Michigan 48824, United States*

Setare Tahmasebi Nick − *Michigan State University, Department of Chemistry, East Lansing, Michigan 48824, United States*

Alireza Ghanbarpour − *Michigan State University, Department of Chemistry, East Lansing, Michigan 48824, United States*; orcid.org/0000-0002-7485-029X

Hadi Gholami − *Michigan State University, Department of Chemistry, East Lansing, Michigan 48824, United States*; orcid.org/0000-0001-6520-0845

Chrysoula Vasileiou − *Michigan State University, Department of Chemistry, East Lansing, Michigan 48824, United States*

Complete contact information is available at: https://pubs.acs.org/10.1021/jacs.1c05039

Author Contributions

‡These authors contributed equally to this work.

Funding

Generous support was provided by the NIH (GM101353).

Notes

The authors declare no competing financial interest.

ACKNOWLEDGMENTS

All crystallographic data were collected at the Advanced Photon Source, an Office of Science User Facility operated for the US Department of Energy (DOE) Office of Science by Argonne National Laboratory, supported by the US DOE under contract No. DE-AC02-06CH11357. Use of the LS-CAT Sector 21 was supported by the Michigan Economic Development Corporation the Michigan Technology Tri-Corridor (Grant 085P1000817) and the MSU office of the Vice President for Research.

ABBREVIATIONS

QY, Quantum Yield; FP, Fluorescent Protein; NIR, Near Infra-Red; LSS, Large Stokes Shift; ICT, Internal Charge Transfer; ESPT, Excited State Proton Transfer; ESIPT, Excited State Internal Proton Transfer; SB, Schiff Base; PSB, Protonated Schiff Base; hCRBPII, human Cellular Retinol Binding Protein II; Å, angstrom; ε, extinction coefficient; EGFP, enhanced GFP; NLS, Nuclear Localization Sequence; PBS, Phosphate Buffered Saline; PDB, Protein Data Bank; RFP, Red Fluorescent Protein; NES, Nuclear Exclusion Sequence; Abs, Absorption; Em, Emission

REFERENCES

(1) (a) Chudakov, D. M.; Matz, M. V.; Lukyanov, S.; Lukyanov, K. A. Fluorescent Proteins and Their Applications in Imaging Living Cells and Tissues. *Physiol. Rev.* **2010**, *90*, 1103. (b) Dean, K. M.; Palmer, A. E. Advances in fluorescence labeling strategies for dynamic cellular imaging. *Nat. Chem. Biol.* **2014**, *10*, 512. (c) Guo, Z. Q.; Park, S.; Yoon, J.; Shin, I. Recent progress in the development of near-infrared fluorescent probes for bioimaging applications. *Chem. Soc. Rev.* **2014**, *43*, 16. (d) Hilderbrand, S. A.; Weissleder, R. Near-infrared fluorescence: application to in vivo molecular imaging. *Curr. Opin. Chem. Biol.* **2010**, *14*, 71. (e) Kowada, T.; Maeda, H.; Kikuchi, K. BODIPY-based probes for the fluorescence imaging of biomolecules in living cells. *Chem. Soc. Rev.* **2015**, *44*, 4953. (f) Luo, S. L.; Zhang, E. L.; Su, Y. P.; Cheng, T. M.; Shi, C. M. A review of NIR dyes in cancer targeting and imaging. *Biomaterials* **2011**, *32*, 7127. (g) Nienhaus, K.; Nienhaus, G. U. Fluorescent proteins for live-cell imaging with super-resolution. *Chem. Soc. Rev.* **2014**, *43*, 1088. (h) Schaferling, M. The Art of Fluorescence Imaging with Chemical Sensors. *Angew. Chem., Int. Ed.* **2012**, *51*, 3532. (i) Specht, E. A.; Braselmann, E.; Palmer, A. E. In *Annual Review of Physiology*; Julius, D., Ed.; Annual Reviews: Palo Alto, 2017; Vol. *79*, p 93. (j) Yang, Z. G.; Cao, J. F.; He, Y. X.; Yang, J. H.; Kim, T.; Peng, X. J.; Kim, J. S. Macro-/micro-environment-sensitive chemosensing and biological imaging. *Chem. Soc. Rev.* **2014**, *43*, 4563. (k) Yuan, L.; Lin, W. Y.; Zheng, K. B.; He, L. W.; Huang, W. M. Far-red to near infrared analyte-responsive fluorescent probes based on organic fluorophore platforms for fluorescence imaging. *Chem. Soc. Rev.* **2013**, *42*, 622. (l) Wang, C. S.; Wang, Z. H.; Zhao, T.; Li, Y.; Huang, G.; Sumer, B. D.; Gao, J. M. Optical molecular imaging for tumor detection and image-guided surgery. *Biomaterials* **2018**, *157*, 62.

(2) (a) Day, R. N.; Davidson, M. W. The fluorescent protein palette: tools for cellular imaging. *Chem. Soc. Rev.* **2009**, *38*, 2887. (b) Remington, S. J. Green fluorescent protein: A perspective. *Protein Sci.* **2011**, *20*, 1509. (c) Sample, V.; Newman, R. H.; Zhang, J. The structure and function of fluorescent proteins. *Chem. Soc. Rev.* **2009**, *38*, 2852. (d) Shaner, N. C.; Steinbach, P. A.; Tsien, R. Y. A guide to choosing fluorescent proteins. *Nat. Methods* **2005**, *2*, 905. (e) Wu, B.; Piatkevich, K. D.; Lionnet, T.; Singer, R. H.; Verkhusha, V. V. Modern fluorescent proteins and imaging technologies to study gene expression, nuclear localization, and dynamics. *Curr. Opin. Cell Biol.* **2011**, *23*, 310.

(3) (a) Miller, L. W.; Cai, Y. F.; Sheetz, M. P.; Cornish, V. W. In vivo protein labeling with trimethoprim conjugates: a flexible chemical tag. *Nat. Methods* **2005**, *2*, 255. (b) Sun, Y.; Weliky, D. P. C-13-C-13 Correlation Spectroscopy of Membrane-Associated Influenza Virus Fusion Peptide Strongly Supports a Helix-Turn-Helix Motif and Two Turn Conformations. *J. Am. Chem. Soc.* **2009**, *131*, 13228. (c) Griffin, B. A.; Adams, S. R.; Jones, J.; Tsien, R. Y. Fluorescent labeling of recombinant proteins in living cells with FlAsH. *Methods Enzymol.* **2000**, *327*, 565. (d) Hori, Y.; Kikuchi, K. Protein labeling with fluorogenic probes for no-wash live-cell imaging of proteins. *Curr. Opin. Chem. Biol.* **2013**, *17*, 644. (e) Keppler, A.; Gendreizig, S.; Gronemeyer, T.; Pick, H.; Vogel, H.; Johnsson, K. A general method for the covalent labeling of fusion proteins with small molecules in vivo. *Nat. Biotechnol.* **2003**, *21*, 86. (f) Loving, G. S.;

Sainlos, M.; Imperiali, B. Monitoring protein interactions and dynamics with solvatochromic fluorophores. *Trends Biotechnol.* **2010**, *28*, 73. (g) Zhang, J.; Campbell, R. E.; Ting, A. Y.; Tsien, R. Y. Creating new fluorescent probes for cell biology. *Nat. Rev. Mol. Cell Biol.* **2002**, *3*, 906. (h) Dahlberg, P. D.; Sartor, A. M.; Wang, J. R.; Saurabh, S.; Shapiro, L.; Moerner, W. E. Identification of PAmKate as a Red Photoactivatable Fluorescent Protein for Cryogenic Super-Resolution Imaging. *J. Am. Chem. Soc.* **2018**, *140*, 12310. (i) Fu, Y. X.; Han, H. H.; Zhang, J. J.; He, X. P.; Feringa, B. L.; Tian, H. Photocontrolled Fluorescence "Double-Check" Bioimaging Enabled by a Glycoprobe-Protein Hybrid. *J. Am. Chem. Soc.* **2018**, *140*, 8671. (j) Jun, J. V.; Petersson, E. J.; Chenoweth, D. M. Rational Design and Facile Synthesis of a Highly Tunable Quinoline-Based Fluorescent Small-Molecule Scaffold for Live Cell Imaging. *J. Am. Chem. Soc.* **2018**, *140*, 9486. (k) Zhang, Y.; Song, K. H.; Tang, S. C.; Ravelo, L.; Cusido, J.; Sun, C.; Zhang, H. F.; Raymo, F. M. Far-Red Photoactivatable BODIPYs for the Super-Resolution Imaging of Live Cells. *J. Am. Chem. Soc.* **2018**, *140*, 12741. (l) Murrey, H. E.; Judkins, J. C.; am Ende, C. W.; Ballard, T. E.; Fang, Y.; Riccardi, K.; Di, L.; Guilmette, E. R.; Schwartz, J. W.; Fox, J. M.; Johnson, D. S. Systematic Evaluation of Bioorthogonal Reactions in Live Cells with Clickable Halo Tag Ligands: Implications for Intracellular Imaging. *J. Am. Chem. Soc.* **2015**, *137*, 11461. (m) Xu, W.; Zeng, Z. B.; Jiang, J. H.; Chang, Y. T.; Yuan, L. Discerning the Chemistry in Individual Organelles with Small-Molecule Fluorescent Probes. *Angew. Chem., Int. Ed.* **2016**, *55*, 13658.

(4) (a) Shcherbakova, D. M.; Verkhusha, V. V. Near-infrared fluorescent proteins for multicolor in vivo imaging. *Nat. Methods* **2013**, *10*, 751. (b) Shcherbo, D.; Shemiakina, I. I.; Ryabova, A. V.; Luker, K. E.; Schmidt, B. T.; Souslova, E. A.; Gorodnicheva, T. V.; Strukova, L.; Shidlovskiy, K. M.; Britanova, O. V.; Zaraisky, A. G.; Lukyanov, K. A.; Loschenov, V. B.; Luker, G. D.; Chudakov, D. M. Near-infrared fluorescent proteins. *Nat. Methods* **2010**, *7*, 827.

(5) Sobhy, M. A.; Elshenawy, M. M.; Takahashi, M.; Whitman, B. H.; Walter, N. G.; Hamdan, S. M. Versatile single-molecule multi-color excitation and detection fluorescence setup for studying biomolecular dynamics. *Rev. Sci. Instrum.* **2011**, *82*, 113702.

(6) (a) Chen, Y. H.; Zhao, J. Z.; Guo, H. M.; Xie, L. J. Geometry Relaxation-Induced Large Stokes Shift in Red-Emitting Borondipyrromethenes (BODIPY) and Applications in Fluorescent Thiol Probes. *J. Org. Chem.* **2012**, *77*, 2192. (b) Jiang, M. J.; Gu, X. G.; Lam, J. W. Y.; Zhang, Y. L.; Kwok, R. T. K.; Wong, K. S.; Tang, B. Z. Two-photon AIE bio-probe with large Stokes shift for specific imaging of lipid droplets. *Chem. Sci.* **2017**, *8*, 5440. (c) Qi, Y.; Huang, Y.; Li, B. W.; Zeng, F.; Wu, S. Z. Real-Time Monitoring of Endogenous Cysteine Levels In Vivo by near-Infrared Turn-on Fluorescent Probe with Large Stokes Shift. *Anal. Chem.* **2018**, *90*, 1014. (d) Butkevich, A. N.; Lukinavicius, G.; D'Este, E.; Hell, S. W. Cell-Permeant Large Stokes Shift Dyes for Transfection-Free Multicolor Nanoscopy. *J. Am. Chem. Soc.* **2017**, *139*, 12378.

(7) (a) Zhao, L. H.; He, X.; Huang, Y. B.; Li, J. L.; Li, Y. L.; Tao, S.; Sun, Y.; Wang, X. H.; Ma, P. Y.; Song, D. Q. A novel ESIPT-ICT-based near-infrared fluorescent probe with large stokes-shift for the highly sensitive, specific, and non-invasive in vivo detection of cysteine. *Sens. Actuators, B* **2019**, *296*, 126571. (b) Zhu, M. Q.; Xu, Y. M.; Sang, L. F.; Zhao, Z. Y.; Wang, L. J.; Wu, X. Q.; Fan, F. G.; Wang, Y.; Li, H. An ICT-based fluorescent probe with a large Stokes shift for measuring hydrazine in biological and water samples. *Environ. Pollut.* **2020**, *256*, 113427. (c) Dahal, D.; McDonald, L.; Pokhrel, S.; Paruchuri, S.; Konopka, M.; Pang, Y. A NIR-emitting cyanine with large Stokes shifts for live cell imaging: large impact of the phenol group on emission. *Chem. Commun.* **2019**, *55*, 13223. (d) Peng, X. J.; Song, F. L.; Lu, E.; Wang, Y. N.; Zhou, W.; Fan, J. L.; Gao, Y. L. Heptamethine cyanine dyes with a large stokes shift and strong fluorescence: A paradigm for excited-state intramolecular charge transfer. *J. Am. Chem. Soc.* **2005**, *127*, 4170. (e) Wu, Y. Y.; Chen, Y.; Gou, G. Z.; Mu, W. H.; Lv, X. J.; Du, M. L.; Fu, W. F. Large Stokes Shift Induced by Intramolcular Charge Transfer in N,O-Chelated Naphthyridine-BF2 Complexes. *Org. Lett.* **2012**, *14*, 5226. (f) Hu, R. R.; Gomez-Duran, C. F. A.; Lam, J. W. Y.; Belmonte-Vazquez, J. L.; Deng, C. M.; Chen, S. J.; Ye, R. Q.; Pena-Cabrera, E.; Zhong, Y. C.; Wong, K. S.; Tang, B. Z. Synthesis, solvatochromism, aggregation-induced emission and cell imaging of tetraphenylethene-containing BODIPY derivatives with large Stokes shifts. *Chem. Commun.* **2012**, *48*, 10099. (g) Greiner, R.; Schlucker, T.; Zgela, D.; Langhals, H. Fluorescent aryl naphthalene dicarboximides with large Stokes shifts and strong solvatochromism controlled by dynamics and molecular geometry. *J. Mater. Chem. C* **2016**, *4*, 11244.

(8) (a) Aparin, I. O.; Sergeeva, O. V.; Mishin, A. S.; Khaydukov, E. V.; Korshun, V. A.; Zatsepin, T. S. Excimer-FRET Cascade in Dual DNA Probes: Open Access to Large Stokes Shift, Enhanced Acceptor Light up, and Robust RNA Sensing. *Anal. Chem.* **2020**, *92*, 7028. (b) Conlon, P.; Yang, C. Y. J.; Wu, Y. R.; Chen, Y.; Martinez, K.; Kim, Y. M.; Stevens, N.; Marti, A. A.; Jockusch, S.; Turro, N. J.; Tan, W. H. Pyrene excimer signaling molecular beacons for probing nucleic acids. *J. Am. Chem. Soc.* **2008**, *130*, 336. (c) Kim, T. I.; Jin, H. Y.; Bae, J.; Kim, Y. Excimer Emission-Based Fluorescent Probe Targeting Caspase-3. *Anal. Chem.* **2017**, *89*, 10565.

(9) (a) Sie, E. J.; McIver, J.; Lee, Y. H.; Fu, L.; Kong, J.; Gedik, N. Valley-selective optical Stark effect in monolayer WS2. *Nat. Mater.* **2015**, *14*, 290. (b) Stokker-Cheregi, F.; Vinattieri, A.; Feltin, E.; Simeonov, D.; Levrat, J.; Carlin, J. F.; Butte, R.; Grandjean, N.; Gurioli, M. Impact of quantum confinement and quantum confined Stark effect on biexciton binding energy in GaN/AlGaN quantum wells. *Appl. Phys. Lett.* **2008**, *93*, 152105.

(10) (a) Piatkevich, K. D.; Malashkevich, V. N.; Almo, S. C.; Verkhusha, V. V. Engineering ESPT Pathways Based on Structural Analysis of LSSmKate Red Fluorescent Proteins with Large Stokes Shift. *J. Am. Chem. Soc.* **2010**, *132*, 10762. (b) Piatkevich, K. D.; Hulit, J.; Subach, O. M.; Wu, B.; Abdulla, A.; Segall, J. E.; Verkhusha, V. V. Monomeric red fluorescent proteins with a large Stokes shift. *Proc. Natl. Acad. Sci. U. S. A.* **2010**, *107*, 5369. (c) Yang, J.; Wang, L.; Yang, F.; Luo, H. M.; Xu, L. L.; Lu, J. L.; Zeng, S. Q.; Zhang, Z. H. mBeRFP, an Improved Large Stokes Shift Red Fluorescent Protein. *PLoS One* **2013**, *8*, e64849. (d) Chu, J.; Oh, Y.; Sens, A.; Ataie, N.; Dana, H.; Macklin, J. J.; Laviv, T.; Welf, E. S.; Dean, K. M.; Zhang, F. J.; Kim, B. B.; Tang, C. T.; Hu, M.; Baird, M. A.; Davidson, M. W.; Kay, M. A.; Fiolka, R.; Yasuda, R.; Kim, D. S.; Ng, H. L.; Lin, M. Z. A bright cyan-excitable orange fluorescent protein facilitates dual-emission microscopy and enhances bioluminescence imaging in vivo. *Nat. Biotechnol.* **2016**, *34*, 760. (e) Shcherbakova, D. M.; Hink, M. A.; Joosen, L.; Gadella, T. W. J.; Verkhusha, V. V. An Orange Fluorescent Protein with a Large Stokes Shift for Single-Excitation Multicolor FCCS and FRET Imaging. *J. Am. Chem. Soc.* **2012**, *134*, 7913.

(11) (a) Sedgwick, A. C.; Wu, L. L.; Han, H. H.; Bull, S. D.; He, X. P.; James, T. D.; Sessler, J. L.; Tang, B. Z.; Tian, H.; Yoon, J. Excited-state intramolecular proton-transfer (ESIPT) based fluorescence sensors and imaging agents. *Chem. Soc. Rev.* **2018**, *47*, 8842. (b) Zhao, J. Z.; Ji, S. M.; Chen, Y. H.; Guo, H. M.; Yang, P. Excited state intramolecular proton transfer (ESIPT): from principal photophysics to the development of new chromophores and applications in fluorescent molecular probes and luminescent materials. *Phys. Chem. Chem. Phys.* **2012**, *14*, 8803.

(12) (a) Weller, A. Quantitative Untersuchungen der Fluoreszenzumwandlung bei Naptholen. *Zeitschrift Fur Elektrochemie* **1952**, *56*, 662. (b) Weller, A. Fast Reactions of Excited Molecules. *Prog. React. Kinet. Mech.* **1961**, *1*, 187.

(13) (a) Li, C. Z.; Yang, Y. G.; Ma, C.; Liu, Y. F. Effect of amino group on the excited-state intramolecular proton transfer (ESIPT) mechanisms of 2-(2 '-hydroxyphenyl)benzoxazole and its amino derivatives. *RSC Adv.* **2016**, *6*, 5134. (b) Padalkar, V. S.; Tathe, A.; Gupta, V. D.; Patil, V. S.; Phatangare, K.; Sekar, N. Synthesis and Photo-Physical Characteristics of ESIPT Inspired 2-Substituted Benzimidazole, Benzoxazole and Benzothiazole Fluorescent Derivatives. *J. Fluoresc.* **2012**, *22*, 311. (c) Li, C. Z.; Ma, C.; Li, D. L.; Liu, Y. F. Excited state intramolecular proton transfer (ESIPT) of 6-amino-2-(2 '-hydroxyphenyl)benzoxazole in dichloromethane and methanol: A

https://doi.org/10.1021/jacs.1c05039
J. Am. Chem. Soc. 2021, 143, 15091−15102

TD-DFT quantum chemical study. *J. Lumin.* **2016**, *172*, 29. (d) Chung, M. W.; Lin, T. Y.; Hsieh, C. C.; Tang, K. C.; Fu, H.; Chou, P. T.; Yang, S. H.; Chi, Y. Excited-State Intramolecular Proton Transfer (ESIPT) Fine Tuned by Quinoline-Pyrazole Isomerism: pi-Conjugation Effect on ESIPT. *J. Phys. Chem. A* **2010**, *114*, 7886. (e) Liu, B.; Wang, J. F.; Zhang, G.; Bai, R. K.; Pang, Y. Flavone-Based ESIPT Ratiometric Chemodosimeter for Detection of Cysteine in Living Cells. *ACS Appl. Mater. Interfaces* **2014**, *6*, 4402. (f) Zheng, D. Y.; Zhang, M. Z.; Zhao, G. J. Combined TDDFT and AIM Insights into Photoinduced Excited State Intramolecular Proton Transfer (ESIPT) Mechanism in Hydroxyl-and Amino-Anthraquinone Solution. *Sci. Rep.* **2017**, *7*, 10.

(14) (a) Leiderman, P.; Genosar, L.; Huppert, D. Excited-state proton transfer: Indication of three steps in the dissociation and recombination process. *J. Phys. Chem. A* **2005**, *109*, 5965. (b) Spry, D. B.; Fayer, M. D. Proton Transfer and Proton Concentrations in Protonated Nafion Fuel Cell Membranes. *J. Phys. Chem. B* **2009**, *113*, 10210. (c) Liu, W. M.; Han, F. Y.; Smith, C.; Fang, C. Ultrafast Conformational Dynamics of Pyranine during Excited State Proton Transfer in Aqueous Solution Revealed by Femtosecond Stimulated Raman Spectroscopy. *J. Phys. Chem. B* **2012**, *116*, 10535. (d) Premont-Schwarz, M.; Barak, T.; Pines, D.; Nibbering, E. T. J.; Pines, E. Ultrafast Excited-State Proton-Transfer Reaction of 1-Naphthol-3,6-Disulfonate and Several 5-Substituted 1-Naphthol Derivatives. *J. Phys. Chem. B* **2013**, *117*, 4594. (e) Han, F. Y.; Liu, W. M.; Fang, C. Excited-state proton transfer of photoexcited pyranine in water observed by femtosecond stimulated Raman spectroscopy. *Chem. Phys.* **2013**, *422*, 204.

(15) (a) Sheng, W.; Nairat, M.; Pawlaczyk, P. D.; Mroczka, E.; Farris, B.; Pines, E.; Geiger, J. H.; Borhan, B.; Dantus, M. Ultrafast Dynamics of a "Super" Photobase. *Angew. Chem., Int. Ed.* **2018**, *57*, 14742. (b) Lahiri, J.; Moemeni, M.; Kline, J.; Borhan, B.; Magoulas, I.; Yuwono, S. H.; Piecuch, P.; Jackson, J. E.; Dantus, M.; Blanchard, G. J. Proton Abstraction Mediates Interactions between the Super Photobase FR0-SB and Surrounding Alcohol Solvent. *J. Phys. Chem. B* **2019**, *123*, 8448.

(16) (a) Wang, W. J.; Nossoni, Z.; Berbasova, T.; Watson, C. T.; Yapici, I.; Lee, K. S. S.; Vasileiou, C.; Geiger, J. H.; Borhan, B. Tuning the Electronic Absorption of Protein-Embedded All-trans-Retinal. *Science* **2012**, *338*, 1340. (b) Sheng, W.; Nick, S. T.; Santos, E. M.; Ding, X. L.; Zhang, J.; Vasileiou, C.; Geiger, J. H.; Borhan, B. A Near-Infrared Photoswitchable Protein-Fluorophore Tag for No-Wash Live Cell Imaging. *Angew. Chem., Int. Ed.* **2018**, *57*, 16083. (c) Santos, E. M.; Berbasova, T.; Wang, W. J.; Salmani, R. E.; Sheng, W.; Vasileiou, C.; Geiger, J. H.; Borhan, B. Engineering of a Red Fluorogenic Protein/Merocyanine Complex for Live-Cell Imaging. *ChemBioChem* **2020**, *21*, 723. (d) Yapici, I.; Lee, K. S. S.; Berbasova, T.; Nosrati, M.; Jia, X. F.; Vasileiou, C.; Wang, W. J.; Santos, E. M.; Geiger, J. H.; Borhan, B. "Turn-On" Protein Fluorescence: In Situ Formation of Cyanine Dyes. *J. Am. Chem. Soc.* **2015**, *137*, 1073. (e) Ghanbarpour, A.; Nairat, M.; Nosrati, M.; Santos, E. M.; Vasileiou, C.; Dantus, M.; Borhan, B.; Geiger, J. H. Mimicking Microbial Rhodopsin Isomerization in a Single Crystal. *J. Am. Chem. Soc.* **2019**, *141*, 1735. (f) Ghanbarpour, A.; Pinger, C.; Esmatpour Salmani, R.; Assar, Z.; Santos, E. M.; Nosrati, M.; Pawlowski, K.; Spence, D.; Vasileiou, C.; Jin, X.; Borhan, B.; Geiger, J. H. Engineering the hCRBPII Domain-Swapped Dimer into a New Class of Protein Switches. *J. Am. Chem. Soc.* **2019**, *141*, 17125. (g) Nosrati, M.; Berbasova, T.; Vasileiou, C.; Borhan, B.; Geiger, J. H. A Photoisomerizing Rhodopsin Mimic Observed at Atomic Resolution. *J. Am. Chem. Soc.* **2016**, *138*, 8802.

(17) (a) Diwu, Z.; Lu, Y. X.; Zhang, C. L.; Klaubert, D. H.; Haugland, R. P. Fluorescent molecular probes 0.2. The synthesis, spectral properties and use of fluorescent solvatochromic Dapoxyl-(TM) dyes. *Photochem. Photobiol.* **1997**, *66*, 424. (b) Min, J.; Lee, J. W.; Ahn, Y. H.; Chang, Y. T. Combinatorial dapoxyl dye library and its application to site selective probe for human serum albumin. *J. Comb. Chem.* **2007**, *9*, 1079. (c) Ando, Y.; Homma, Y.; Hiruta, Y.; Citterio, D.; Suzuki, K. Structural characteristics and optical properties of a series of solvatochromic fluorescent dyes displaying long-wavelength emission. *Dyes Pigm.* **2009**, *83*, 198.

(18) Storch, J.; Corsico, B. The emerging functions and mechanisms of mammalian fatty acid-binding proteins. *Annu. Rev. Nutr.* **2008**, *28*, 73.

(19) Berbasova, T.; Nosrati, M.; Vasileiou, C.; Wang, W.; Lee, K. S. S.; Yapici, I.; Geiger, J. H.; Borhan, B. Rational Design of a Colorimetric pH Sensor from a Soluble Retinoic Acid Chaperone. *J. Am. Chem. Soc.* **2013**, *135*, 16111.

(20) (a) Lee, K. S. S.; Berbasova, T.; Vasileiou, C.; Jia, X. F.; Wang, W. J.; Choi, Y.; Nossoni, F.; Geiger, J. H.; Borhan, B. Probing Wavelength Regulation with an Engineered Rhodopsin Mimic and a C15-Retinal Analogue. *ChemPlusChem* **2012**, *77*, 273. (b) Crist, R. M.; Vasileiou, C.; Rabago-Smith, M.; Geiger, J. H.; Borhan, B. Engineering a rhodopsin protein mimic. *J. Am. Chem. Soc.* **2006**, *128*, 4522.

(21) (a) Gao, F.; Gao, T.; Zhou, K. C.; Zeng, W. B. Small Molecule-Photoactive Yellow Protein Labeling Technology in Live Cell Imaging. *Molecules* **2016**, *21*, 1163. (b) Kumar, N.; Hori, Y.; Nishiura, M.; Kikuchi, K. Rapid no-wash labeling of PYP-tag proteins with reactive fluorogenic ligands affords stable fluorescent protein conjugates for long-term cell imaging studies. *Chem. Sci.* **2020**, *11*, 3694. (c) Leng, S.; Qiao, Q. L.; Miao, L.; Deng, W. G.; Cui, J. N.; Xu, Z. C. A wash-free SNAP-tag fluorogenic probe based on the additive effects of quencher release and environmental sensitivity. *Chem. Commun.* **2017**, *53*, 6448. (d) Sun, X. L.; Zhang, A. H.; Baker, B.; Sun, L.; Howard, A.; Buswell, J.; Maurel, D.; Masharina, A.; Johnsson, K.; Noren, C. J.; Xu, M. Q.; Correa, I. R. Development of SNAP-Tag Fluorogenic Probes for Wash-Free Fluorescence Imaging. *ChemBioChem* **2011**, *12*, 2217.

https://doi.org/10.1021/jacs.1c05039
J. Am. Chem. Soc. 2021, 143, 15091−15102